

## High resolution synchrotron X-ray investigation of carbon dioxide evolution in operating direct methanol fuel cells

Christoph Hartnig<sup>1\*</sup>, Ingo Manke<sup>2,3</sup>, Jana Schloesser<sup>2</sup>, Philipp Krüger<sup>1</sup>, Robert Kuhn<sup>1</sup>, Heinrich Rieseemeier<sup>4</sup>, Klaus Wippermann<sup>5</sup>, John Banhart<sup>2</sup>

<sup>1</sup>Zentrum für Sonnenenergie- und Wasserstoff-Forschung Ulm, Helmholtzstr. 8, 89081 Ulm, Germany

<sup>2</sup>Helmholtz Zentrum für Materialien und Energie, Glienicker Str. 100, 14109 Berlin, Germany

<sup>3</sup>Technische Universität Berlin, Hardenberg Str. 36, 10623 Berlin

<sup>4</sup>Federal Institute for Materials Research and Testing, Unter den Eichen 87, 12205 Berlin, Germany

<sup>5</sup>Forschungszentrum Jülich GmbH, 52425 Jülich, Germany

\*corresponding author: christoph.hartnig@basf.com

present address: BASF Fuel Cell GmbH, Industriepark Höchst G865, 65926 Frankfurt/Main, Germany, phone: +49/69/305 41514

### Abstract

The carbon dioxide evolution and bubble formation in an operating fuel has been studied by means of synchrotron X-ray radiography. Two different observation directions have been chosen: a through plane insight has been employed to track the formation of bubbles starting at the corner of the lands of the flow field; a depth profile of the carbon dioxide evolution has been derived from cross sectional studies describing an affected area of up to 100  $\mu\text{m}$ . The dynamics of the bubble formation and detachment of the bubbles from the position of formation is strongly correlated with the current density. Below a threshold value, a minimum gas pressure has to be achieved before the bubble formation starts in the flow field channel; beyond the threshold value a continuous bubbling and removal of the bubbles is observed. Cracks and breaks in the catalyst layer which result from the preparation process are visible under operating conditions and a possible swelling of the catalyst layer is not sufficient to close the open spots.

**Keywords:** DMFC, carbon dioxide evolution, synchrotron radiography, in situ study, cross section, through plane

## 1. Introduction

In terms of fuel storage and transport, direct methanol fuel cells (DMFCs) offer a great solution for future energy supply. Power densities in the range of 100 up to 300 mW cm<sup>-2</sup> were reported for DMFCs with active fuel supply at typical operating temperatures around 70°C<sup>1,2</sup>. For passive DMFCs, where no active pumping of methanol solution is employed, lower power densities in the range of 40-50 mW cm<sup>-2</sup> with a 5M MeOH solution have been reported<sup>3</sup>.

The reaction in a DMFC can be split to the anodic oxidation of methanol,  $\text{CH}_3\text{OH} + \text{H}_2\text{O} \rightarrow 6\text{e}^- + 6\text{H}^+ + \text{CO}_2$  and the cathodic oxygen reduction  $3/2 \text{O}_2 + 6\text{e}^- + 6\text{H}^+ \rightarrow 3 \text{H}_2\text{O}$ , leading to an overall reaction of methanol to form water and carbon dioxide, which has a limited solubility in the aqueous phase. As the anodic fuel is usually provided as aqueous solution, gas bubbles might lead to blocked channels and the transport and further fuel supply are stopped. Several approaches have been followed to study the pattern of bubble formation in fuel cells. In the most common approach, the anodic flow field is manufactured of transparent material allowing for a direct visualization of the pattern formation under operating conditions<sup>4,5</sup>. The extension of gas slugs is thereby depending on the employed material and the flow velocity and lead to contradictory results: even for slow flow velocities no slug formation has been observed [4], whereas in a different study the opposite behavior has been reported [5], however, a channel blocking has not been observed. In either case, the wetting characteristics of the transparent material are different from the conventional graphite composite plates as used in state of the art fuel cells which lead to varying results. The carbon dioxide transport, evolution rate and the concentration have also been subject to theoretical studies<sup>6,7,8</sup>. The main focus is thereby set on the concentration distribution and influence of the carbon dioxide partial pressure on the performance of the DMFC.

The preparation of the catalyst layer and structural influences on the performance has been studied with regard on optimization and reduction of crack formation<sup>9,10,11</sup>. Almost independent of the preparation method, small cracks and ruptures occurring during the drying of the catalyst ink or paste, can be detected *ex situ* on the finished electrode.

Common to the studies of carbon dioxide formation and investigations of the structure of the catalyst layer is a missing insight employing an unperturbed fuel cell setup under operating conditions.

In this study, we report on investigations of the carbon dioxide evolution and bubble formation excluding any modifications which might lead to unpredictable artifacts. A standard cell was employed to observe evolution and transport processes by means of synchrotron radiography. Technical details are explained in the following section; in section 3 the carbon dioxide formation is highlighted; the structure of the catalyst layer under operating conditions is elucidated in more detail in section 4.

## 2. Technical details

The experiments were performed at the tomography facility of the Helmholtz Centre Berlin (formerly Hahn-Meitner Institute Berlin) and the Federal Institute of Materials Research and Testing (BAM), the BAMline, which is located at the synchrotron source BESSY in Berlin (Germany). A 4008x2672 pixel<sup>2</sup> camera setup (PCO 4000 with a CdWO scintillator screen) was used to capture image area sizes of up to 8×8 mm<sup>2</sup> with pixel sizes between 1 and 2 μm and a physical spatial resolution of typically 2-5 μm. A W-Si multilayer monochromator with an energy resolution of about  $\Delta E/E = 10^{-2}$  was used to obtain a monochromatic X-ray beam with energies around 18 keV. Typical measurement time per image was around 1-4 s (exposure time).

Two different flow field structures have been used; a threefold serpentine flow field for the through plane studies and a single channel geometry for the in-plane investigations which were both machined in graphite composite plates. An in-house prepared MEA based on Nafion 115 has been hot pressed on an catalyst coated gas carbon cloth gas diffusion media with a platinum catalyst on the cathodic electrode (loading: 2.5 mg/cm<sup>2</sup>) and a platinum/ruthenium catalyst (loading: 2.0 mg/cm<sup>2</sup>) on the anodic electrode. The stack was operated at a temperature of 75°C at a cathodic utilization rate  $u_c$  of 50% ( $\lambda=2$ ) and a humidified air stream (dew point  $T_D=60^\circ\text{C}$ ). The methanol was supplied as 1 M aqueous solution; the over-stoichiometric flow rate was adjusted in a way to allow for a rapid removal of the formed carbon dioxide bubbles. For the study of the evolution patterns, the flow had been reduced to a

minimum level in order to keep the cell voltage constant and ensure on the other hand the formation of sufficiently large gas bubbles.

### **3. Carbon dioxide evolution, bubble formation**

Two different viewing directions have been chosen to study the evolution of carbon dioxide evolution, the through plane and the cross sectional viewing direction. The first approach allows for an on-top (through plane) observation of the electrochemically active area. A clear differentiation between areas under the land and under the channels of the serpentine flow field can be made. In Figure 1 different stages of bubble formation can be distinguished: marked with a white arrow is the initial formation at the boundary between the channel and the land of the flow field. Larger bubbles to the left and the right of the marked position which did not yet collapse to form a large trunk and are almost blocking the complete channel cross section can be identified. The apparent 'pseudo-overlap' of the bubbles with the wall of the reactant channels results from the slightly tilted walls of the gas channels. A removal step where the bubbles are shoved away is not included in the image.

Contrary to the through plane orientation which only gives a summarized representation of the MEA and the anodic and cathodic gas diffusion media, in the cross sectional view one can distinguish the different components. Based on this differentiation, the evolution and transport of primary bubbles in the porous media can be detected and the consecutive growth of the gas bubble can be followed. In Figure 2 a series of consecutive images describing the formation of a gas bubble is displayed. In the circled area the slow evolution of a larger bubble can be followed. As the time distance between the images is around 6 seconds, the complete process of bubble formation until the separation from the surface takes up to 50 sec (at the employed current density of 60 mA/cm<sup>2</sup>).

The time dependence of the gas evolution has been investigated in more details function of the employed current density. Therefore, the gas content (resp. the absorption) of a specific area covering the involved region of the diffusion media and the channel has been studied. In Figure 3 the evaluated area covering diffusion media and the reactant channel is outlined. A direct correlation of the two regions is not attempted but the time dependence of the gas content is followed. At low current

densities, two filling 'modes' can be detected (left part of Figure 4): after the electric load is switched on, the gas content increases up to a threshold level followed by a sudden decay (detachment of the gas bubble) and a subsequent switch back to the gas satisfied situation. At a higher current density ( $i_0=30 \text{ mA/cm}^2$ , right half of Figure 4), a different, cyclic behavior describing a continuous filling and emptying of the considered area was found. Furthermore, the continuous (instead of sudden) increase and spontaneous decrease of the absorption illustrates the continuous bubble growth instead of the sudden eruption of a carbon dioxide bubble as observed at lower current densities. The chosen current density of  $i_0=20 \text{ mA/cm}^2$  appears to be a threshold value from the sudden bubble formation to the periodic bubble growth and bubble detachment. Besides a change in the transport mechanism, an increase in the frequency of bubble formation can be observed which however is obvious from the increase of the current density.

The influence of the structural properties especially of the woven materials has been taken into closer account imaging the bubble formation from a cross sectional viewing direction. In Figure 5a the anodic flow field channel and the adjacent diffusion media are displayed. The dark areas describe open space in the diffusion media where the gas bubbles which cannot evolve from the cloth are 'stored'. The same pattern is found in a through plane view (Figure 5b) which resembles the formation of gas troughs under the bends of the cloth. As can be seen from a comparison with an SEM image, the periodicity of the structure of the diffusion media is reflected in the maxima of the absorption distribution; the maximum-to-maximum distance of  $500 \text{ }\mu\text{m}$  is identical to the structure as observable in the SEM image (Figure 5c). Close to the position of the crossings of the fiber strands no gas agglomerations can be found which indicates these spots as outlets for gas bubbles.

#### **4. Structural properties of the catalyst layer**

As mentioned in the introductory section, the morphology of the anodic and cathodic catalyst layer has been subject of investigations with regard on crack formation and influence of morphology on performance. The fate of the cracks as appearing during the drying of the MEA and their influence and role in the carbon dioxide formation has not been elucidated so far.

In Figure 6, an enlarged area of the catalytically active area under operating conditions is displayed. The persistence of cracks can be easily identified which excludes a speculated swelling of the catalyst layer (due to the present polymer content) leading to a closure of the breaks even after several hours of operation. As the cracked spots appear brighter than the surrounding area, an increased gas content in these areas seems very likely.

A direct correlation of the place of evolution of the gas bubbles in the channels (compare to Figure 1 and explanations above) and larger cracks in the catalyst layer cannot be drawn based on the images presented here; on the other hand, a contribution of slits and enlarged pores on the surface to the bubble evolution and detachment is very probable as these spots represent channels for enhanced gas migration. Due to a still existing resolution limit, questions concerning the mesostructure of the catalyst layer under operating condition cannot be answered.

## **5. Discussion/Conclusion**

The carbon dioxide evolution and transport in unmodified fuel cells has been studied employing realistic operating conditions. The initial formation of gas bubbles starts at the edge of the reactant channel and the diffusion media at open spaces of the diffusion media result from intersections of the woven material. At low current densities, the gas pressure is increased inside the diffusion media leading to sudden eruptions of gas bubbles which are shoved away after some time. From a threshold value of  $20 \text{ mA/cm}^2$  onwards a cyclic eruptive behavior was found which has been observed in a similar manner in low temperature polymer electrolyte fuel cells where liquid water droplets evolve on the same place across the diffusion media and evaporate<sup>12,13</sup>. The catalyst layer keeps its structure under operating conditions: scratches and breaks which result from the manufacturing process are still visible whereas a general differentiation between water and gas filled spots cannot be made based on the obtained images.

In conclusion, synchrotron imaging gives insight in processes which are not accessible by other techniques. The formation of gas bubbles as well as the structure of the catalyst layer in an unperturbed setup have been described for the first time. Due to the high temporal resolution, even dynamic processes taking place under operating conditions can be visualized in a unique way.

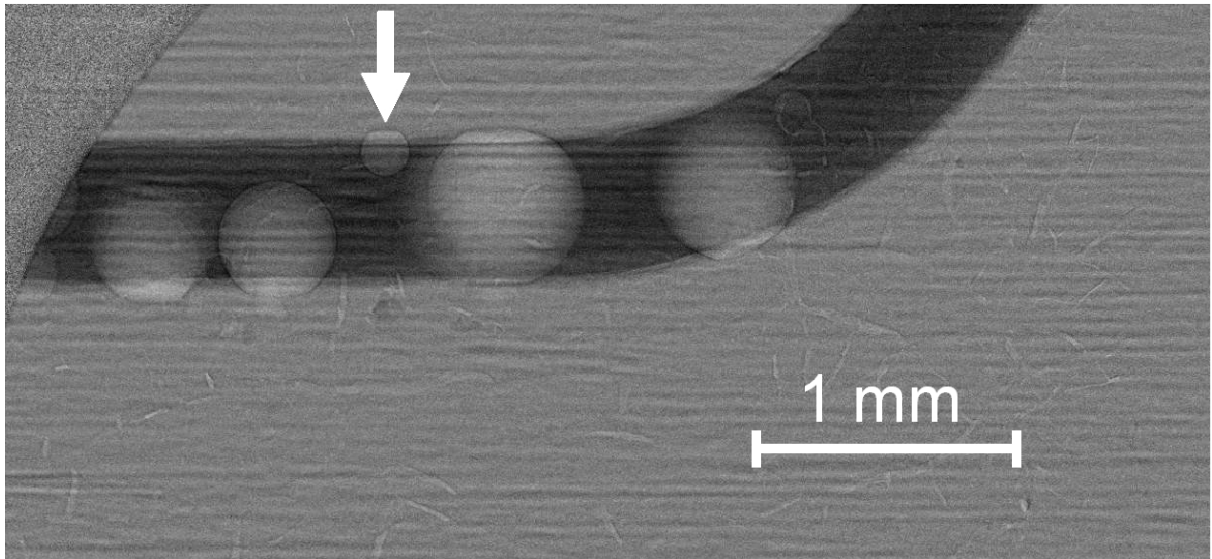


Figure 1: On top view of the carbon dioxide formation in the channels of the flow field. The bubble formation starts preferably at the channel edges as marked by the arrow ( $i_0=60 \text{ mA/cm}^2$ ).

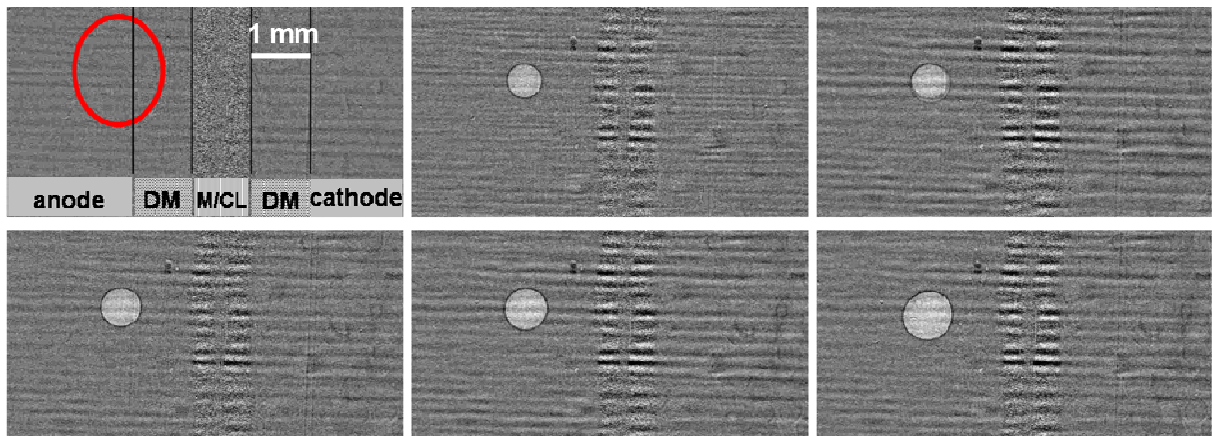


Figure 2: Time-dependence of the bubble formation on the interface between the GDL and the channel of the flow field (in-plane view). The red circle denotes the active spot at which the bubble formation has been observed; image-to-image time: 6 sec ( $i_0=60 \text{ mA/cm}^2$ ).

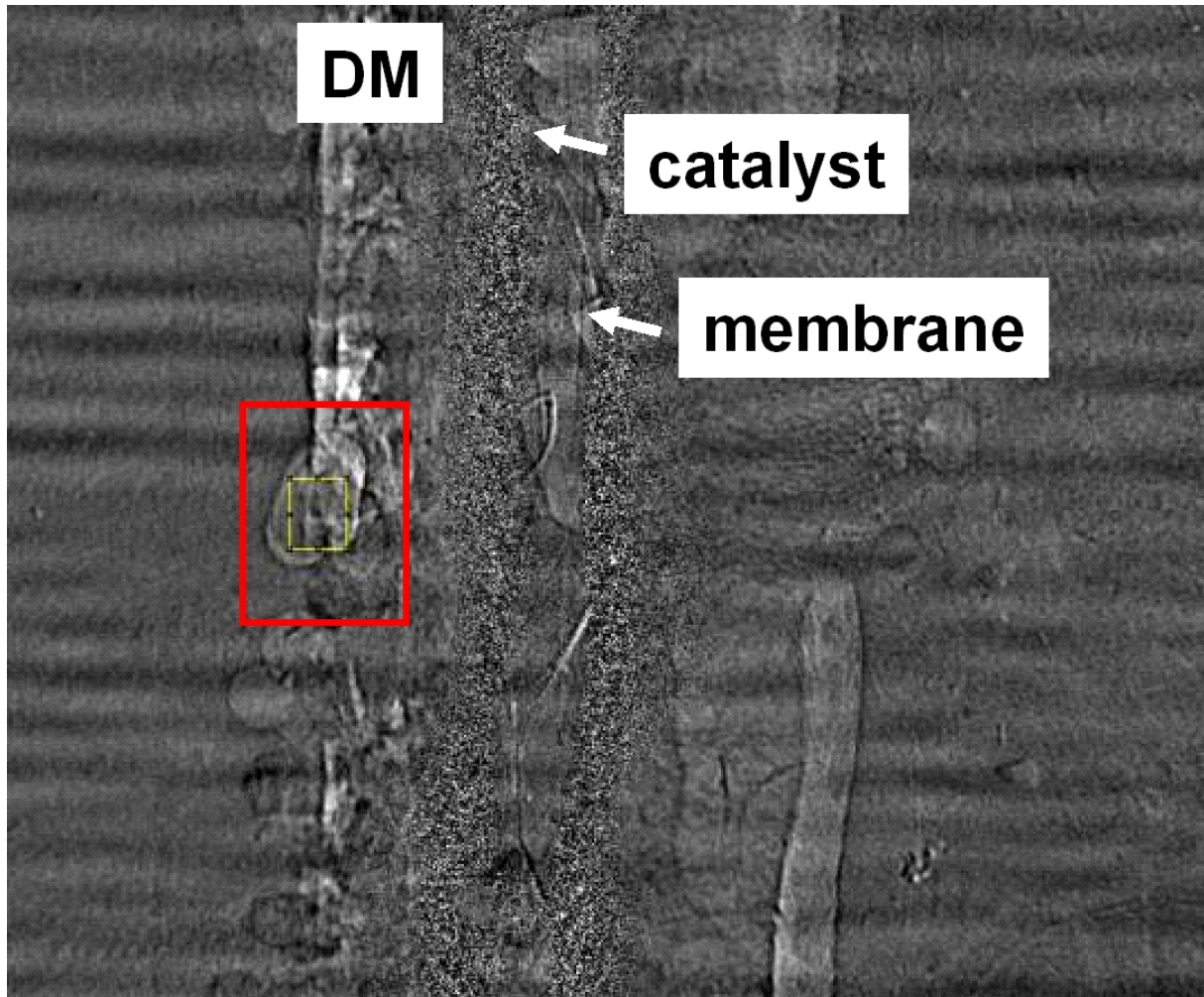


Figure 3: Area considered for the quantification of the gas content inside the diffusion media and the reactant channel (cross sectional view).

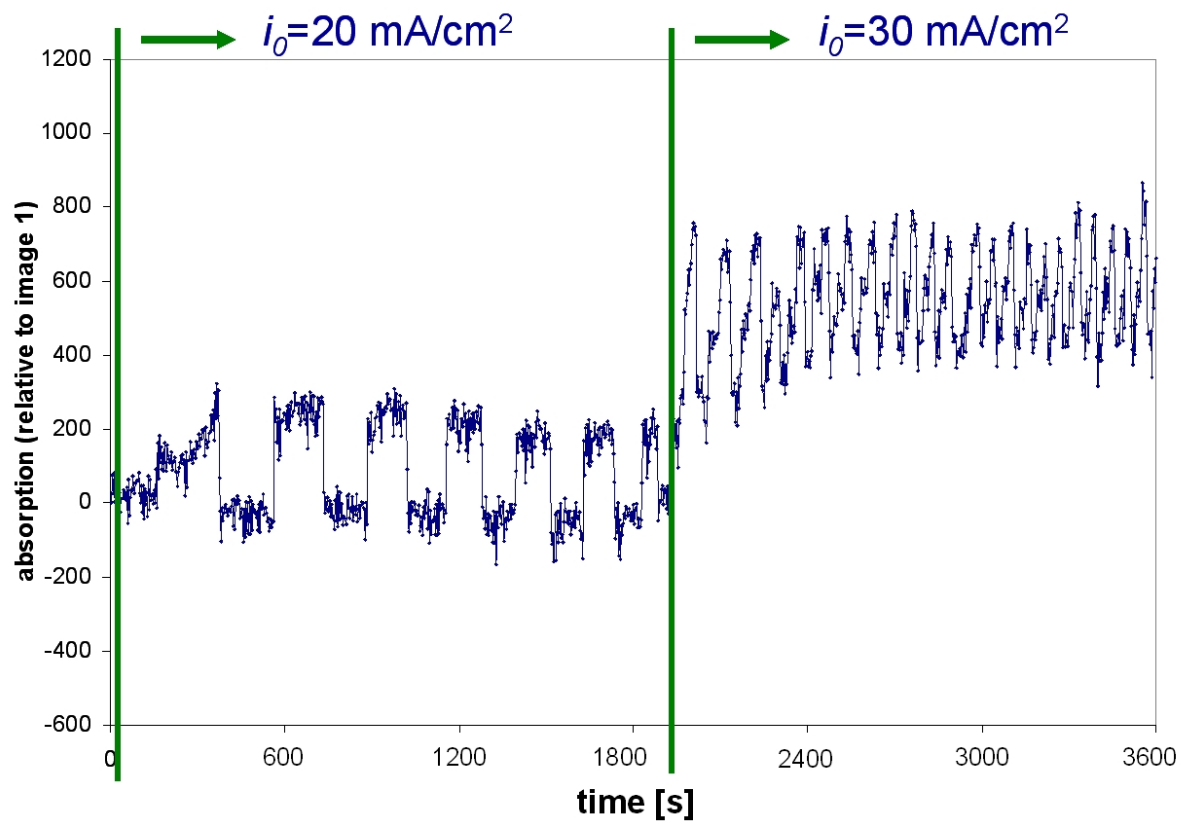


Figure 4: Gas content of the area outlined in Figure 3. At low current densities (left side), two filling stages can be distinguished; at higher current densities (right side) a cyclic filling and emptying of the considered area is observed.

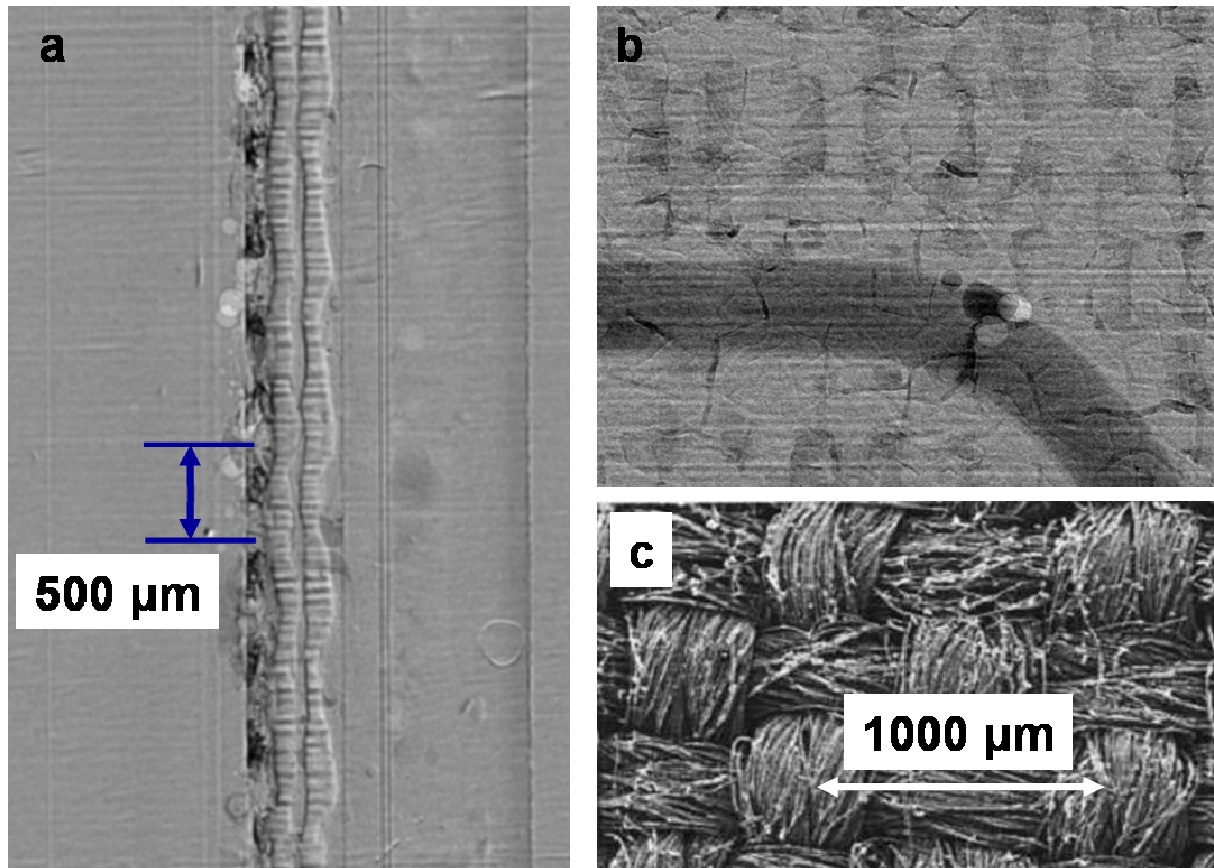
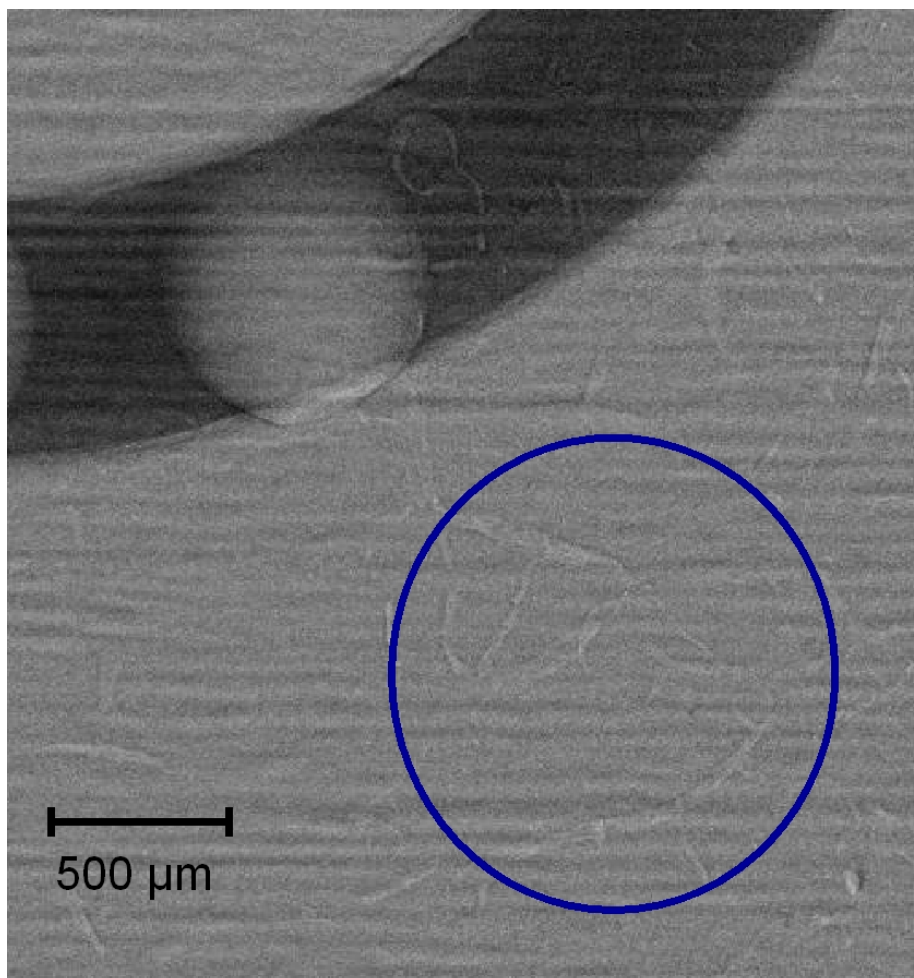


Figure 5: a: Visualization of gas agglomerations in the anodic diffusion media by means of cross sectional imaging. The structure of the diffusion media is reflected in the maxima of the absorption coefficient. b: Through plane view of the gas agglomerations which reside in the bends of the carbon cloth. c: SEM-image of a woven diffusion media.



**Figure 6: Structure of the catalyst layer under operating conditions. The highlighted area is located under the ribs of the anodic and cathodic flow fields. Cracks and scratches resulting from the preparation of the catalyst layer (doctor blading) are persistent and are not vanishing by the slight swelling of the catalyst.**

## References

- 
- <sup>1</sup> T. V. Reshetenko, H.-T. Kim, H. Lee, M. Jang, Ho-Jin Kweon, *J. Power Sources* 160 (2006) 925-932
  - <sup>2</sup> K. Scott, W.M. Taama, J. Cruickshank, *J. Power Sources* 65 (1997) 159-171
  - <sup>3</sup> B. Bae, B. K. Kho, T.-H. Lim, I.-H. Oh, S.-A. Hong, H. Y. Ha, *J. Power Sources* 158 (2006) 1256-1261
  - <sup>4</sup> P. Argyropoulos, K. Scott, W.M. Taama, *Electrochim. Acta* 44 (1999) 3575-3584
  - <sup>5</sup> H. Yang, T.S. Zhao, Q. Ye, *J. Power Sources* 139 (2005) 79-90
  - <sup>6</sup> A.A. Kulikovskiy, *Electrochim. Acta* 51 (2006) 2003-2011
  - <sup>7</sup> Z. H. Wang, C.-Y. Wang, *J. Electrochem. Soc.* 150 (2003) A508-A519
  - <sup>8</sup> E.S. Gaddis, A. Vogelpohl, *Chem. Eng. Sci.* 41 (1986) 97-105
  - <sup>9</sup> Z. Wang, Y. Liu, V. M. Linkov, *J. Power Sources* 160 (2006) 326-333
  - <sup>10</sup> F. Liu, C.-Y. Wang, *Electrochim. Acta* 52 (2006) 1417-1425

---

<sup>11</sup> Ch. Hartnig, L. Jörissen, W. Lehnert, J. Scholta, *Materials for fuel cells*, Chapter 5, ed. M. Gasik, Woodhead Publishing, Cambridge, 2008

<sup>12</sup> I. Manke, Ch. Hartnig, M. Grünerbel, W. Lehnert, N. Kardjilov, A. Haibel, A. Hilger, J. Banhart, H. Riesemeier, *Appl. Phys. Lett.* 90 (2007) 174105

<sup>13</sup> Ch. Hartnig, I. Manke, R. Kuhn, N. Kardjilov, J. Banhart, W. Lehnert, *Appl. Phys. Lett.* 92 (2008) 134106